

# Implementation of the Natural Mode Analysis for Nanotopologies Using a Volumetric Method of Moments (V-MoM) Algorithm

Volume 6, Number 4, August 2014

Xuezhi Zheng, Student Member, IEEE

Ventsislav K. Valev

Niels Verellen

Vladimir Volskiy, Member, IEEE

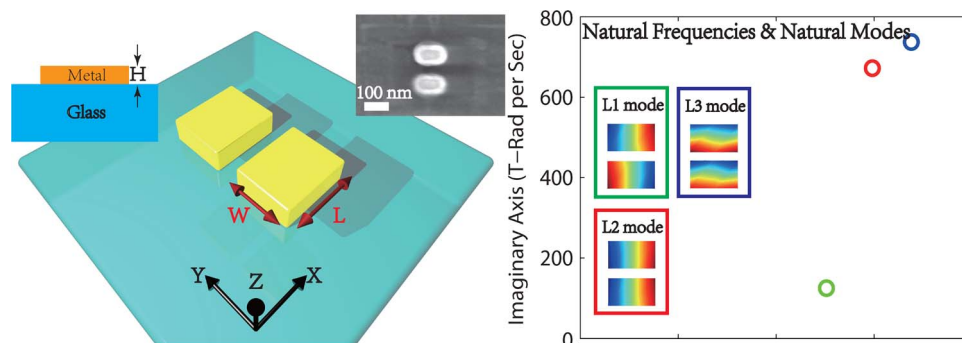
Lars O. Herrmann

Pol Van Dorpe

Jeremy J. Baumberg

Guy A. E. Vandenbosch, Fellow, IEEE

V. V. Moschchalkov



DOI: 10.1109/JPHOT.2014.2331236

1943-0655 © 2014 IEEE

# Implementation of the Natural Mode Analysis for Nanotopologies Using a Volumetric Method of Moments (V-MoM) Algorithm

Xuezhi Zheng,<sup>1</sup> *Student Member, IEEE*, Ventsislav K. Valev,<sup>2</sup>  
Niels Verellen,<sup>3,4</sup> Vladimir Volskiy,<sup>1</sup> *Member, IEEE*, Lars O. Herrmann,<sup>2</sup>  
Pol Van Dorpe,<sup>4,5</sup> Jeremy J. Baumberg,<sup>2</sup>  
Guy A. E. Vandenbosch,<sup>1</sup> *Fellow, IEEE*, and V. V. Moschchalkov<sup>3</sup>

<sup>1</sup> Department of Electrical Engineering (ESAT-TELEMIC), KU Leuven, 3001 Leuven, Belgium  
<sup>2</sup> NanoPhotonics Centre, Cavendish Laboratory, Department of Physics, University of Cambridge, Cambridge CB30HE, U.K.  
<sup>3</sup> Institute for Nanoscale Physics and Chemistry (INPAC), Katholieke Universiteit Leuven (KUL), 3001 Leuven, Belgium  
<sup>4</sup> IMEC, 3001 Leuven, Belgium  
<sup>5</sup> Department of Physics and Astronomy, Katholieke Universiteit Leuven (KUL), 3001 Leuven, Belgium

DOI: 10.1109/JPHOT.2014.2331236

1943-0655 © 2014 IEEE. Translations and content mining are permitted for academic research only. Personal use is also permitted, but republication/redistribution requires IEEE permission. See [http://www.ieee.org/publications\\_standards/publications/rights/index.html](http://www.ieee.org/publications_standards/publications/rights/index.html) for more information.

Manuscript received April 16, 2014; revised May 23, 2014; accepted May 23, 2014. Date of publication June 18, 2014; date of current version July 4, 2014. This work was supported in part by the Fund for Scientific Research—Flanders, by the Katholieke Universiteit Leuven (GOA), by the Flemish Government through Methusalem Funding, by the MP1201 COST Action, and by the U.K. EPSRC Grant EP/G060649/1 and ERC LINASS 320503. The work of N. Verellen was supported by the F.W.O. (Flanders). Corresponding author: X. Zheng (e-mail: xuezhi.zheng@esat.kuleuven.be).

**Abstract:** Within the framework of a method-of-moments algorithm, the natural frequencies and natural modes of a scatterer/antenna can be found by looking for the complex frequencies where the determinant of the impedance matrix becomes zero. However, for nanotopologies, the value of this determinant can easily go beyond the resolution or representation limits available on present-day computers. In this work, we propose a substitute for the matrix determinant that avoids this problem altogether: the characteristic term. A robust numerical procedure for locating natural frequencies using this new target function is outlined. Then, the natural frequencies of three different nanostructures, namely, a gold and nickel nanopatch and a gold nanodimer, are calculated and validated by numerically and experimentally obtained scattering/extinction spectra.

**Index Terms:** Plasmonics, nano-antennas, modeling, volumetric method of moments (V-MoM), natural frequencies and natural modes.

## 1. Introduction

Depending on the geometry, material and boundary condition, a mechanical system, e.g., a bridge, drum, molecule, or an atom, has a set of natural (normal) modes. Such a set together with the corresponding natural frequencies characterizes the most intrinsic aspects of the system and determines the system's free and forced response. In electromagnetics, the interests in natural frequencies and natural current modes of a general radiating structure, e.g., scatterers or antennas, arose from the studies on the interaction of a nuclear electromagnetic pulse (EMP)

with metallic objects in the early 1970s [1]. There, scatterers' transient response universally exhibits damped sinusoids, which suggests the existence of natural frequencies in the complex frequency domain where the real and imaginary axes represent the oscillation frequency and the decay rate, respectively [1], [2]. At the natural frequencies, the electric field integral equation (EFIE) [3] that describes the interaction of electromagnetic waves with a radiating object has solutions without any incident electromagnetic field [1]. By utilizing the Method of Moments (MoM) algorithm [4], the electric field integral equation (EFIE) can be reduced to a finite dimensional matrix, i.e., an impedance matrix. The natural frequencies can be numerically determined by the zeros of the determinant of the impedance matrix, which are complex numbers  $\omega_\alpha = \omega_{\alpha r} + j\omega_{\alpha i}$ . The corresponding natural current modes can be subsequently attained at natural frequencies.

Similar ideas can be naturally extended to plasmonic nanoantennas [5], where the natural frequencies and the natural current modes of a nanorod and a dolmen structure are extracted and their roles in determining the line position and the quality factor of surface plasmon resonances are revealed. Akin to its microwave counterparts, since the interaction of free space electromagnetic radiation with a nanoantenna can be in general captured by Maxwell's equations, the EFIE [3] and its Method of Moments (MoM) matrix form [6]–[11] can be established for nanoscatterers. Hence, to locate the natural frequencies of a nanoantenna, looking for the zeros of the impedance matrix's determinant is in general mathematically correct. Nevertheless, difficulties exist in directly applying this principle as a numerical criterion to a topology that generates an impedance matrix with *large* dimension but *small* matrix elements. Take a simple nanobar of dimensions 370 nm in length, 70 nm in width and 50 nm in thickness as an example. To accurately describe the electromagnetic properties, the length is divided by 10 blocks, the width by two blocks and the thickness by two blocks. In total, 164 volumetric basis functions (the matrix dimension) are used. The real and imaginary parts of the matrix element on the diagonal are in the order of  $10^{-15}$  and  $10^{-11}$  respectively, suggesting a determinant in the order of  $10^{-1640}$ , which is far beyond the limit of the double precision representation  $10^{-308}$  [12]. A scaling-up procedure (for example, multiply each row by  $10^{15}$ ) could be a solution to the present problem. However, unless a uniform scaling factor is applied to all the frequency points in the search region (or along the search path), this procedure could disturb the trends to be followed in the behavior of the determinant. However, since the procedure proposed further in the paper completely alleviates this problem, we prefer to keep the original matrix elements, and thus the trend as a function of frequency, as they are.

Second, for all the root-finding algorithms, a good initial estimation or at least a definite region to search is required. At microwave frequencies, an initial guess for the natural frequencies for simple structures like wire antennas, patch antennas, etc., can always be taken from design rules and circuit models [13]. However, due to the fact that metals behave so differently in the optical frequency region, compared to microwaves, these simple models cannot be used anymore. For the topologies of interest in the study of plasmonics, like the star [14], spiral [15], square ring [16], Cross [17], RNDC (ring near disc) [18], V [19], and dolmen [20], [21], there are no simple design rules [22], even in the microwave range.

Therefore, to determine the natural frequencies of a nanoantenna a new parameter is required and, correspondingly, a robust numerical algorithm should be developed. In this work, we propose such a new parameter for nanoantenna applications as a substitute for the determinant. We will refer to this parameter as the characteristic term. Based on the argument principle [23], a numerical way of searching natural frequencies is illustrated. The proposed method is qualitatively verified by experiments.

## 2. Matrix Form of Electric Field Integral Equation (EFIE) and Natural Frequencies of a Nanoantenna

The EFIE is defined in the following functional relation linking the incoming light wave with the induced current flowing in the nanoantenna

$$\mathbf{Z}(\mathbf{J}(\mathbf{r}, \omega)) = \mathbf{E}_{\text{inc}}(\mathbf{r}, \omega) \quad (1)$$

where the functional relation  $Z$  is

$$Z(\mathbf{J}(\mathbf{r}, \omega)) = \frac{\mathbf{J}(\mathbf{r}, \omega)}{j\omega(\varepsilon(\omega) - \varepsilon_0)} + j\omega\mu_0 \int_V \bar{\mathbf{G}}(\mathbf{r}, \mathbf{r}', \omega) \cdot \mathbf{J}(\mathbf{r}', \omega) dv' \quad \mathbf{r}' \in V. \quad (2)$$

In (2), we assume that the nanoantenna is made of a dispersive material of dielectric function  $\varepsilon(\omega)$  occupying a volume of  $V$ .  $\varepsilon_0$  and  $\mu_0$  are the vacuum permittivity and the vacuum permeability.  $\bar{\mathbf{G}}(\mathbf{r}, \mathbf{r}', \omega)$  is the tensor Green's function linking the source current  $\mathbf{J}(\mathbf{r}', \omega)$  at space point  $\mathbf{r}'$  with the electric field at observation point  $\mathbf{r}$ .  $e^{j\omega t}$  is employed as the time convention. For the sake of simplicity, in this paper, the free space Green's function is considered

$$\bar{\mathbf{G}}(\mathbf{r}, \mathbf{r}', \omega) = \left[ \bar{\mathbf{I}} + \frac{1}{k^2} \nabla \nabla \right] g(\mathbf{r}, \mathbf{r}') = \left[ \bar{\mathbf{I}} + \frac{1}{k^2} \nabla \nabla \right] \frac{e^{-jk|\mathbf{r}-\mathbf{r}'|}}{4\pi|\mathbf{r}-\mathbf{r}'|}. \quad (3)$$

In (3),  $\bar{\mathbf{I}}$  is the unit dyad and  $g(\mathbf{r}, \mathbf{r}')$  is the scalar free space Green's function.  $k$  is the complex wave number which is the ratio of a complex frequency  $\omega$  to the speed of light  $c$ . The natural frequency and its corresponding natural mode can be defined as

$$Z(\mathbf{J}(\mathbf{r}, \omega_\alpha)) = \mathbf{0}. \quad (4)$$

In (4), the natural frequency  $\omega_\alpha$  is a complex number  $\omega_{\alpha r} + j\omega_{\alpha i}$  with  $\alpha$  specifying the index of the corresponding natural mode. Within the framework of a Volumetric Method of Moments algorithm (MoM) [6]–[11], we can discretize the continuous body of a scatterer [see Fig. 1(a)] by tetrahedral or hexahedral blocks [see Fig. 1(b) and (c)] and approximate the three dimensional (i.e., volumetric) current flowing in two adjacent blocks with a presumed local current distribution  $\mathbf{f}_n(\mathbf{r})$  (called “a basis function” [4]) and of an amplitude  $j_n(\omega)$ . Especially, in this work we use a three dimensional generalization [9] of the well-known RWG rooftop functions [24], [25]. By further applying a razor blade testing procedure [9], that is, calculating the reactions of a “test function”  $\mathbf{g}_m(\mathbf{r})$  to the electric field generated by a basis function  $\mathbf{f}_n(\mathbf{r})$  and the incident field  $\mathbf{E}_{\text{inc}}(\mathbf{r}, \omega)$  [4], we can approximate the infinitely dimensional operator in Eq. (1) by an  $N$  by  $N$  impedance matrix  $\{z_{mn}(\omega)\}$  in a variational sense

$$\{z_{mn}(\omega)\} \{j_n(\omega)\} = \{e_m(\omega)\} \quad (5)$$

$$z_{mn}(\omega) = \frac{1}{j\omega(\varepsilon(\omega) - \varepsilon_0)} \int_{V_g} \mathbf{g}_m(\mathbf{r}) \cdot \mathbf{f}_n(\mathbf{r}) dv + j\omega\mu_0 \int_{V_g} \mathbf{g}_m(\mathbf{r}) \int_{V_f} \bar{\mathbf{G}}(\mathbf{r}, \mathbf{r}', \omega) \cdot \mathbf{f}_n(\mathbf{r}') dv' dv. \quad (6)$$

In (5),  $\{j_n(\omega)\}$  is a column vector which contains amplitudes of all basis functions and  $\{e_m(\omega)\}$  denotes a column vector whose elements are the reaction of test functions to the incident electric fields. In (6), the integrations span the volumes of the basis function  $V_f$  and the test function  $V_g$ . The detailed evaluation of the highly singular integral kernel (6) is further referred to [9]. Numerically, the natural frequency defined in (4) can be obtained by searching for the complex frequency where (5) has a solution without any excitation,

$$\{z_{mn}(\omega_\alpha)\} \{j_n(\omega_\alpha)\} = \mathbf{0}. \quad (7)$$

In (7), the column vector  $\{j_n(\omega_\alpha)\}$  represents the set of amplitudes of the basis functions at a natural frequency  $\omega_\alpha$ . To assure a non-trivial solution to (7), the determinant of the matrix on its left hand side must be zero

$$\det(\{z_{mn}(\omega_\alpha)\}) = 0. \quad (8)$$

Therefore, the determinant of the impedance matrix is considered as *the parameter*, based on which root finding algorithms, like the contour integral method [26] and the Newton–Raphson method [27], are implemented. Further, after obtaining the corresponding natural

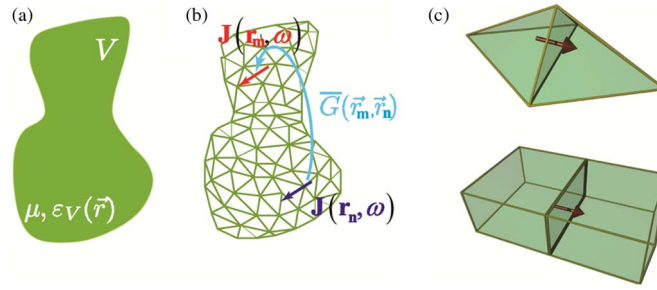


Fig. 1. The discretized representation of a nanoscatterer. (a) The continuous body of an arbitrary nanoscatterer; (b) an illustration of the discretization of the nanoscatterer; (c) and the tetrahedral and hexahedral blocks.

mode vector  $\{j_n(\omega_\alpha)\}$ , we can represent the response of a nanoantenna in frequency domain as [1], [2], [27]

$$\{j_n(\omega)\} = \sum_{\omega_\alpha} \frac{\mathcal{R}(\omega_\alpha)}{j\omega - j\omega_\alpha} \cdot \{\mathbf{e}_m(\omega)\} = \sum_{\omega_\alpha} \frac{\{j_n(\omega_\alpha)\}\{j_n(\omega_\alpha)\}^T}{(j\omega - j\omega_\alpha)} \cdot \{\mathbf{e}_m(\omega)\}. \quad (9)$$

Notice that in (9)  $\mathcal{R}(\omega_\alpha)$  is the residue matrix at a natural frequency  $\omega_\alpha$  and can be decomposed as the outer product of the natural mode vectors  $\{j_n(\omega_\alpha)\}$ . The algebraic order of the natural frequencies is assumed to be one, which is the case for all detected natural frequencies in this work. Further, we refer the readers who are interested in the mathematical background of the expansion in (9) to [28], [29], and the references therein.

### 3. Characteristic Term

In this section, the characteristic term is proposed as a substitute for the matrix determinant used to find natural frequencies. We start with an impedance matrix  $\{z_{mn}(\omega)\}$  containing  $N^2$  elements. This matrix can be triangularized by  $QR$  decomposition [30]

$$\mathbf{Z} = \{z_{mn}(\omega)\} = \mathbf{Q}\mathbf{R} = (\mathbf{q}_1(\omega), \dots, \mathbf{q}_n(\omega)) \begin{pmatrix} u_{11}(\omega) & \cdots & u_{1n}(\omega) \\ & \ddots & \vdots \\ 0 & & u_{nn}(\omega) \end{pmatrix}. \quad (10)$$

In (10),  $\mathbf{Q}$  is a unitary matrix and  $\mathbf{R}$  is an upper triangular matrix. Especially, we construct the  $\mathbf{R}$  matrix in such a way that the diagonal elements of the  $\mathbf{R}$  matrix are always non-negative real numbers. The matrix elements in the  $\mathbf{R}$  matrix are actually the projections of the column vectors in the impedance matrix  $\mathbf{Z}$  onto the column vectors in the unitary matrix  $\mathbf{Q}$ . To find the  $\alpha$ th natural mode whose natural frequency is  $\omega_\alpha$ , we substitute (10) into (7)

$$\mathbf{Q}\mathbf{R}\mathbf{J}(\omega_\alpha) = \mathbf{Q} \begin{pmatrix} u_{11}(\omega_\alpha) & \cdots & u_{1n}(\omega_\alpha) \\ & \ddots & \vdots \\ 0 & & u_{nn}(\omega_\alpha) \end{pmatrix} \begin{pmatrix} j_1(\omega_\alpha) \\ \vdots \\ j_n(\omega_\alpha) \end{pmatrix} = \begin{pmatrix} 0 \\ \vdots \\ 0 \end{pmatrix} \quad (11)$$

where  $j_n(\omega_\alpha)$  represents the amplitude of the  $n$ th basis function at a natural frequency  $\omega_\alpha$ . It can be immediately seen from (11) that if  $u_{nn}(\omega_\alpha)$  is zero, (11) has a non-trivial solution. This fact can be confirmed by evaluating the determinant of the  $\mathbf{Z}$  matrix. Since  $\det(\mathbf{Z}) = \det(\mathbf{Q}) \cdot \det(\mathbf{R})$  and the determinant of a triangular matrix is the product of its diagonal elements, if  $u_{nn}(\omega_\alpha)$  is zero, the determinant of the  $\mathbf{R}$  matrix is zero and thus the determinant of the  $\mathbf{Z}$  matrix is zero. Since the last column in the impedance matrix becomes linearly dependent on the first  $n - 1$  columns, the matrix has one degree of freedom and by imposing a unit amplitude to  $j_n(\omega_\alpha)$ , the

normal mode vector can be solved. Further, the normal mode vector is normalized in such a way that its outer product is the residue matrix  $\mathcal{R}(\omega_\alpha)$  as in (9). However, it must be noticed that the condition that  $u_{nn}(\omega_\alpha) = 0$  is only a sufficient but not a necessary condition for the matrix determinant to be zero. That is, the matrix determinant being zero does not necessarily guarantee that the last element on the diagonal of the  $\mathbf{R}$  matrix is zero. To see this, we interchange the  $m^{\text{th}}$  ( $m = 1, \dots, n$ ) column with the last column in the  $\mathbf{Z}$  matrix, which generates  $n$  equivalent linear systems to (11)

$$\mathbf{R}^{(m)} \mathbf{J}^{(m)}(\omega_\alpha) = \begin{pmatrix} u_{11}^{(m)}(\omega_\alpha) & \cdots & \cdots & u_{1n}^{(m)}(\omega_\alpha) \\ & \ddots & & \vdots \\ & & \ddots & \vdots \\ 0 & & & u_{nn}^{(m)}(\omega_\alpha) \end{pmatrix} \begin{pmatrix} j_1(\omega_\alpha) \\ \vdots \\ j_n(\omega_\alpha) \\ \vdots \\ j_m(\omega_\alpha) \end{pmatrix} = \begin{pmatrix} 0 \\ \vdots \\ \vdots \\ \vdots \\ 0 \end{pmatrix}. \quad (12)$$

Here, the  $\mathbf{Q}$  matrix is dropped by simultaneously left-multiplying the conjugate transpose of the  $\mathbf{Q}$  matrix on both sides of (12). The superscript  $m$  in (12) specifies which column is exchanged with the last column. Notice that the equation in the last row of (12) is

$$u_{nn}^{(m)}(\omega_\alpha) j_m(\omega_\alpha) = 0. \quad (13)$$

To solve (13), two different situations have to be distinguished. When  $u_{nn}^{(m)}(\omega_\alpha)$  is zero, (13) has a nontrivial solution, i.e.,  $j_m(\omega_\alpha)$  has a non-zero value, suggesting that the corresponding basis function is an *active* basis function for the  $\alpha$ th natural mode. On the contrary, when  $u_{nn}(\omega_\alpha) \neq 0$ , the solution  $j_m(\omega_\alpha)$  to (13) is zero and therefore the  $m$ th basis function is an *inactive* basis function for the  $\alpha$ th natural mode. Clearly,  $u_{nn}(\omega_\alpha)$  associated with an *active* basis function for the  $\alpha$ th natural mode is an eligible substitute for the determinant and hereafter referred to as **the characteristic term**.

#### 4. Searching for Natural Frequencies

In this section, by utilizing the determinant of the  $\mathbf{Q}$  matrix in (10) and the proposed characteristic term, we demonstrate the procedure to find the natural frequencies of a nanoantenna. Since the free space Green's function is analytic in the complex frequency plane except at the origin [due to the  $1/k^2$  term in (2)], the entries [as presented in (6)] and the determinant of an impedance matrix are analytic functions of the complex frequency  $\omega$ , except at zero frequency [31]. Consequently, in the frequency range of interest (optical frequencies), the argument principle [23], [26] can be applied to the determinant to find the number of zeros in a given region in the complex plane. That is, since  $f(\omega) = \det(\{z_{mn}(\omega)\})$  is an analytic function in a given domain  $D$  of the complex plane circumscribed by a closed contour  $C$ , the number of zeros can be found by calculating the *logarithmic residue* of  $f(\omega)$  [23], [26], [31]

$$\frac{1}{2\pi j} \oint_C \frac{f'(\omega)}{f(\omega)} d\omega = \frac{\nabla_C \arg(f(\omega))}{2\pi} = N_{\text{zero}}. \quad (14)$$

The contour integral in the leftmost part of (14) is the logarithmic residue and the integral is calculated along the closed contour  $C$  on which  $f(\omega)$  is analytic and nonzero. The contour's positive direction is defined in such a way that when we walk along the positive direction of the contour, the domain  $D$  is always on our left-hand side.  $\nabla_C \arg(f(\omega))$  is the phase-angle change of  $f(\omega)$  after circling around the integration contour  $C$ . Further dividing  $\nabla_C \arg(f(\omega))$  by  $2\pi$  gives the number of zeros within the domain  $D$ . Notice that to determine the number of zeros in a given domain  $D$ , (14) only needs the information on the determinant's phase angle. Though in general the exact numerical value of the determinant is difficult to be represented by the

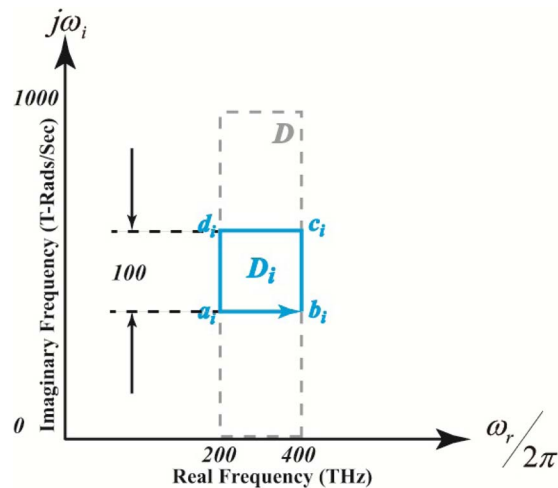


Fig. 2. Domain  $D$  (gray dashed rectangle) in the complex frequency plane. Subdomain  $D_i$  and its waypoints  $a_i$ ,  $b_i$ ,  $c_i$ , and  $d_i$  are highlighted by the cyan color, with its positive direction denoted by the arrow pointing from  $a_i$  to  $b_i$ .

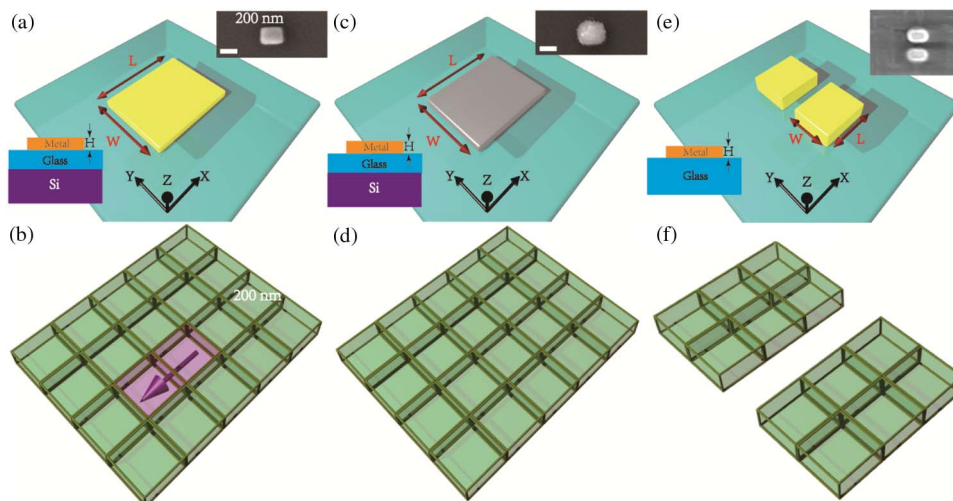


Fig. 3. Gold (Au) nanopatch, nickel (Ni) nanopatch, and gold (Au) nanodimer. The dimensions are for the Au and Ni Nanopatches:  $L = 250$  nm,  $W = 200$  nm,  $H = 25$  nm, and for the Au nanodimer:  $L = 135$  nm,  $W = 100$  nm,  $H = 50$  nm,  $\text{Gap} = 20$  nm). Their depth profiles and SEM images are shown in the insets of (a), (c), and (e). The meshes employed in the calculations are presented in (b), (d), and (f). The magenta arrow in (b) denotes the active basis functions (an X-directed current) whose characteristic term is utilized in the search for the natural frequencies. (a) Au Nanopatch. (b) Mesh for Au Nanopatch. (c) Ni Nanopatch. (d) Mesh for Ni Nanopatch. (e) Au Dimer. (f) Mesh for Au Dimer.

double-precision format, the phase angle information can be retrieved from the  $\mathbf{Q}$  matrix in (10). On one hand, since the diagonal elements of the  $\mathbf{R}$  matrix are pure real and non-negative, the determinant of the  $\mathbf{R}$  matrix gives the amplitude of the determinant of the impedance matrix. On the other hand, due to the fact that the  $\mathbf{Q}$  matrix is a unitary matrix (i.e.,  $|\det(\mathbf{Q})| = 1$ ), the determinant of the  $\mathbf{Q}$  matrix provides the phase angle of the determinant of the impedance matrix. Thereby, by evaluating the determinant of the  $\mathbf{Q}$  matrix around the contour  $C$ , the number of enclosed zeros can be readily found.

We can immediately apply the above principles to practical nanostructures. In the complex frequency plane, we consider a rectangular domain  $D$  (see the dashed rectangle in Fig. 2) with

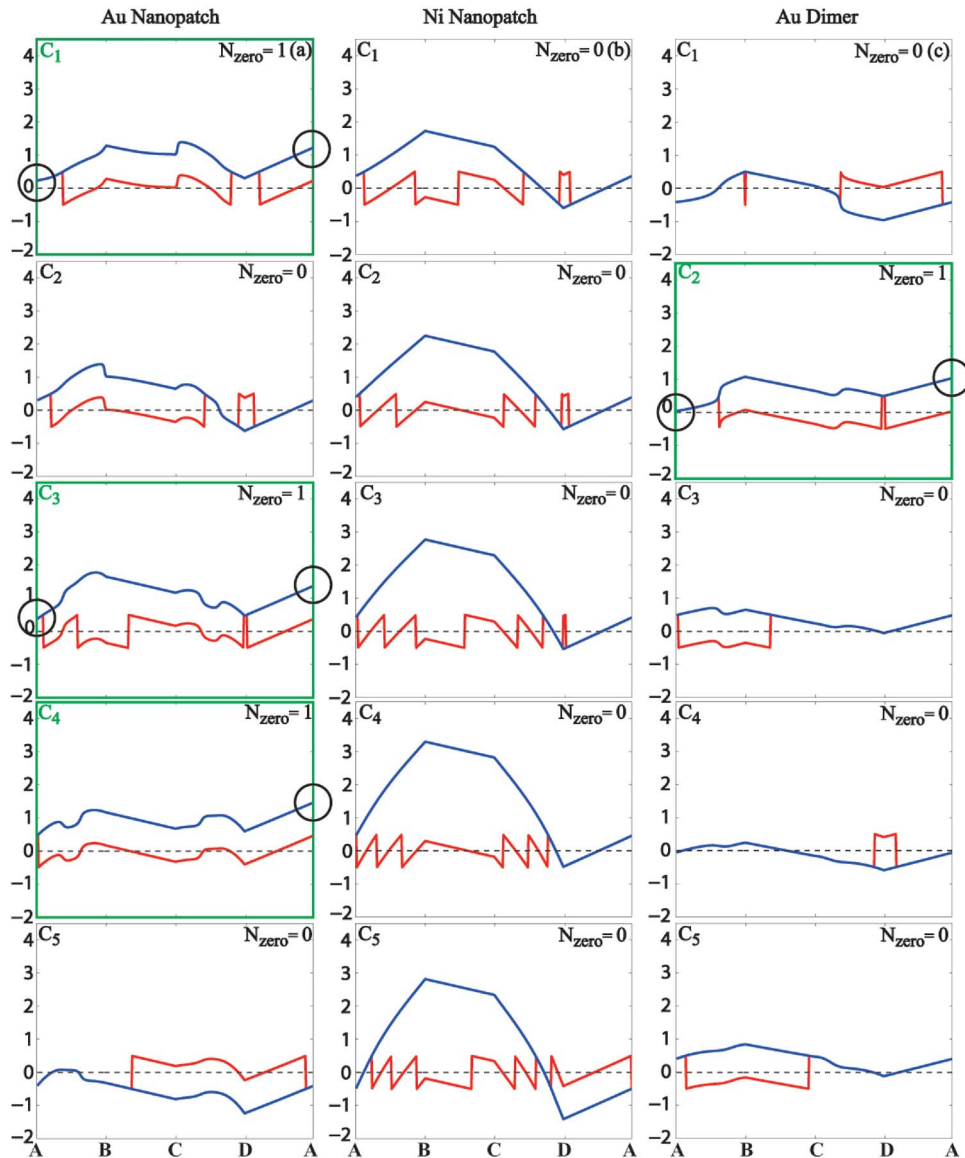


Fig. 4. Phase angles (normalized by  $2\pi$ ) of the determinant of the  $\mathbf{Q}$  matrix along the subdomain contour  $C_i$  ( $i = 1, \dots, 5$ ) for a gold nanopatch (the left column), nickel nanopatch (the middle column), and gold nanodimer (the right column). In (a)–(c), the red and blue curves represent the phase angles without/with the phase jump between adjacent points compensated along the integration contour  $C_i$ , respectively. The figures describing the contours within which zeros exist are highlighted in green.

a width of 200 THz (for the nanopatches, from 200 THz to 400 THz along the real frequency axis; for the nanodimer, from 300 THz to 500 THz along the real frequency axis) and a length of 1000 teraradians per second (from 0 teraradians per second to 1000 teraradians per second along the imaginary frequency axis). By further dividing the domain  $D$  into ten equal subdomains  $D_i$  ( $i = 1, \dots, 10$ ) along the imaginary frequency axis, we calculate the phase angle of the determinant of the  $\mathbf{Q}$  matrix along each subdomain contour  $C_i$  which is defined by four waypoints, i.e.,  $a_i$ ,  $b_i$ ,  $c_i$ , and  $d_i$  (see Fig. 2). The positive direction of the contour is defined as  $a_i \rightarrow b_i \rightarrow c_i \rightarrow d_i$ .

Three nanostructures, i.e., a gold (Au) nanopatch, a nickel (Ni) nanopatch, and a gold (Au) nanodimer, are used as examples. The nanopatches are fabricated on top of a  $\text{SiO}_2$  (100 nm)/Si

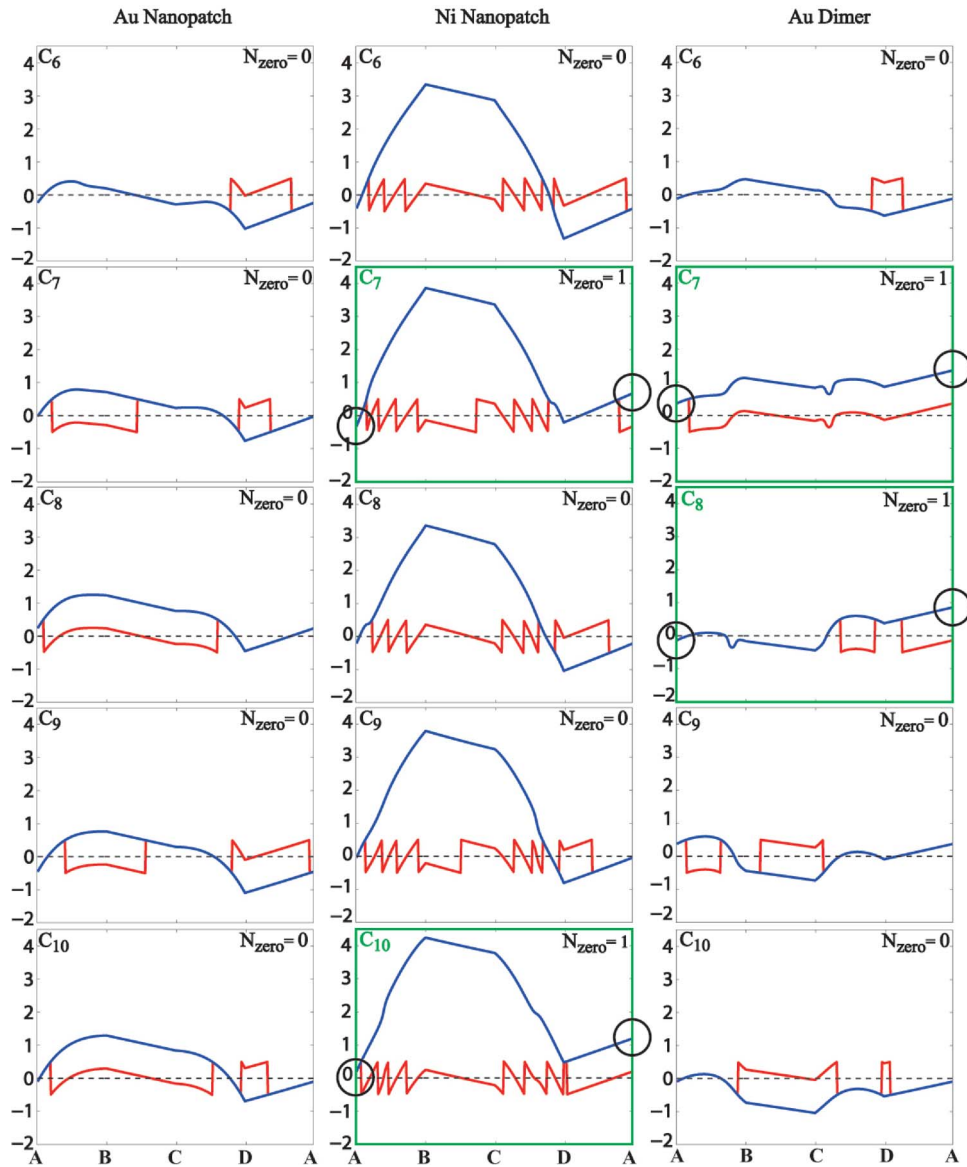


Fig. 5. Phase angles (normalized by  $2\pi$ ) of the determinant of the  $\mathbf{Q}$  matrix along the subdomain contour  $C_i$  ( $i = 6, \dots, 10$ ) for a gold nanopatch (the left column), nickel nanopatch (the middle column), and gold nanodimer (the right column). In (a)–(c), the red and blue curves represent the phase angles with the phase jump between adjacent points compensated along the integration contour  $C_i$ , respectively. The figures describing the contours within which zeros exist are highlighted in green.

layer, while the nanodimer sits on a  $\text{SiO}_2$  substrate. The dimensions, depth profiles and scanning electron microscopy (SEM) image are shown in Fig. 3. In the calculations, the Au and Ni nanopatches are discretized by a mesh with five divisions in X direction, four divisions in Y direction and 1 division in Z direction [panels 3(b,d)], whereas each horizontal slab of the nanodimer is represented by a  $3 \times 2 \times 1$  mesh [panel 3(f)]. Note that a set of finer meshes is also employed in the simulations. Their results are shown in the Supporting Information. The substrate effect is taken into account by assuming a homogeneous surrounding medium with an effective refractive index ( $n = 1.25$ ) in between those of vacuum and glass. The material parameters of gold (Au) and nickel (Ni) as a function of complex frequency are approximated by Drude and Drude–Lorentz models with their parameters shown in the Supporting Information.

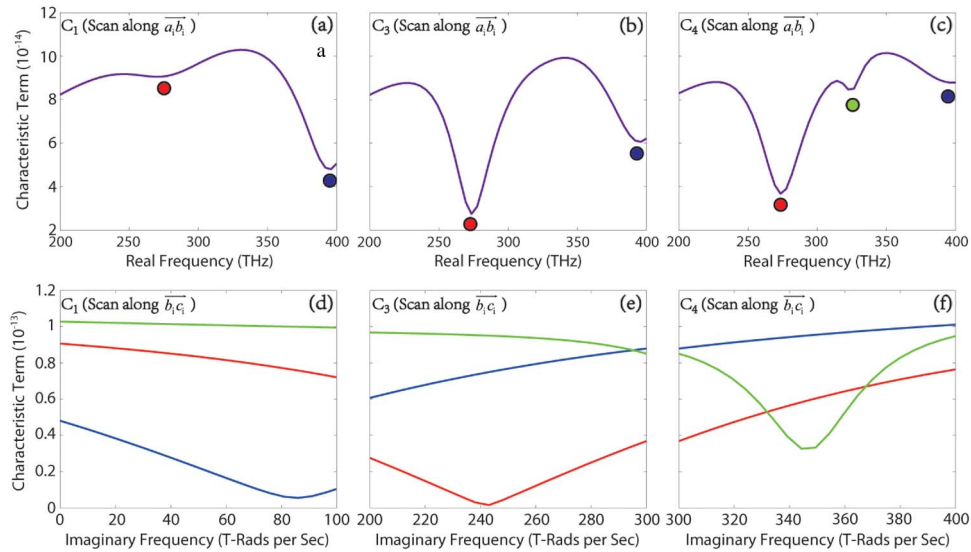


Fig. 6. Estimation of initial guess(es) for the gold nanopatch. In this figure, the characteristic term associated with the basis function denoted by the magenta arrow in Fig. 3 is concerned. In (a)–(c), the characteristic term (the magenta curve) is scanned along the  $a_i b_i$  side of the contours  $C_2$ ,  $C_3$ , and  $C_4$ , with the minima indicated by the color dots. In (d)–(f), the scans, starting from the corresponding color labeled minima in (a)–(c), along the  $b_i c_i$  side are shown.

In Figs. 4 and 5 (for fine mesh, see Figs. S2 and S3 in the Supporting Information), we plot the phase angle change of the determinant of the  $\mathbf{Q}$  matrix around each contour  $C_i$  ( $a_i \rightarrow b_i \rightarrow c_i \rightarrow d_i$ ) for all three structures. Especially, from the panels highlighted in green in Figs. 4(a)–(c) and 5(a)–(c), we can observe that the return phase, i.e., the phase of the determinant of the  $\mathbf{Q}$  matrix after going around the closed contour (indicated with black circles), has a (non-zero multiple of)  $2\pi$  difference from the initial phase, which indicates the existence of zero(s) according to Eq. (14).

Further, the initial guess of the natural frequencies can be performed in two steps: 1) we do all the possible interchanges, collect the terms  $u_{nn}^{(m)}$  and find their minima along the  $a_i b_i$  side of the rectangular domains where zeros rest in. Then, the term [as illustrated for the gold nanopatch in Fig. 6(a)–(c)] which corresponds to the most active basis function [see the basis function denoted by the magenta arrow in Fig. 3(b)] is picked. 2) Take the minima found in step 1) as starting points and scan the same characteristic term along the direction of the  $b_i c_i$  side in each subdomain. If any dips are sought out as in Fig. 6(d)–(f) for the gold nanopatch, make use of the dip position(s) in the complex plane as initial guess(es). By running a root-finding algorithm, such as the Newton–Raphson algorithm [27], Simplex algorithm [32], Differential Evolution algorithm [33], to name a few, we are able to locate the natural frequencies with a certain numerical accuracy. Especially, in this work a frequency point is assumed to give a zero of the determinant if this point results in a characteristic term that is ten thousand times smaller than that of the initial estimation.

The position of numerically located natural frequencies in the complex frequency plane can be confirmed by the calculated scattered/total dissipated (scattered + material loss) power spectra from a V-MoM algorithm [6]–[11] and the experimentally obtained scattering/extinction spectra as shown in Fig. 7(d)–(f) for the three investigated nanoantenna designs. First of all, it can be observed from Fig. 7 that the real part of the natural frequencies determines the line position of resonances with a spectral shift due to the material absorption and radiative loss (see the arrows in Fig. 7). Second, by applying X (Y) polarized light in the simulation [Fig. 7(b)] and unpolarized light in the experiment [Fig. 7(c)], the L1 and L2 mode of the nanopatches are excited. It can be seen from Fig. 7(b) and (c) that both simulations and experiments illustrate that the Ni nanopatch always has a broader resonance than the Au nanopatch, suggesting a lower

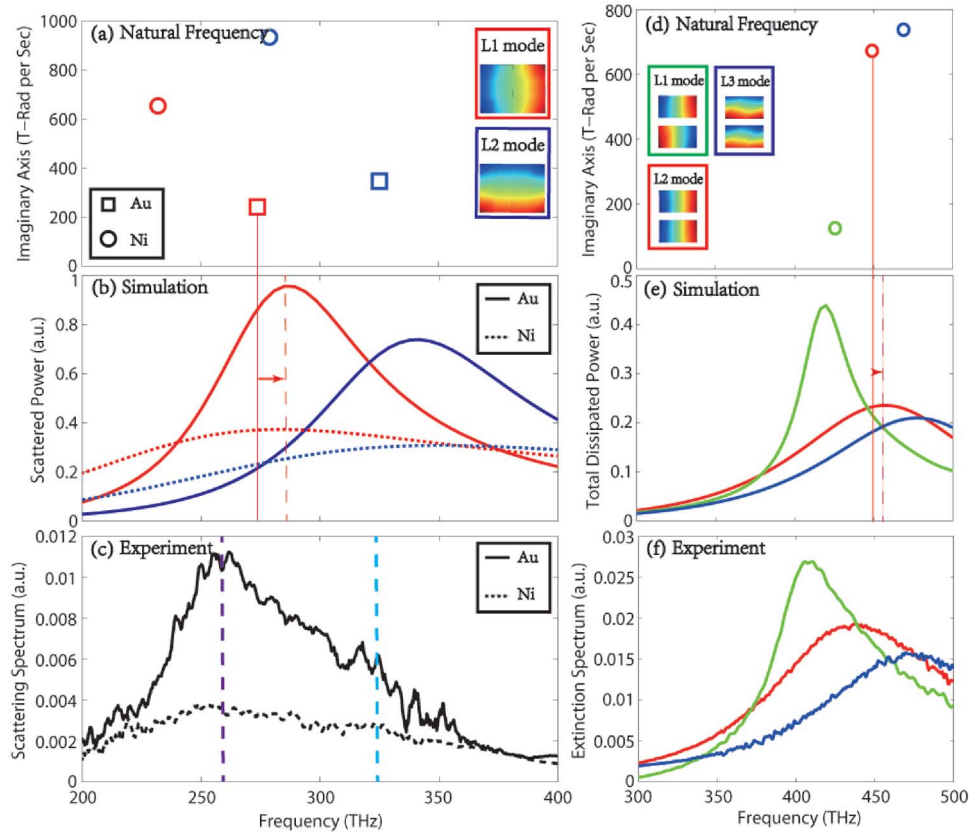


Fig. 7. Natural frequencies, natural modes, and resonances of nanopatches and a nanodimer. (a) The first (L1, in red) and the second (L2, in blue) natural modes (i.e., the mode surface charge distribution with the color coded from blue to red representing the negative and positive charges) and the corresponding natural frequencies (Au: the square marker and Ni: the circle marker) of the nanopatch. In (b), the simulated scattering spectra of the L1 (in red) and L2 (in blue) modes for the Au (the solid line) and Ni (the dashed line) nanopatch are shown. In (c), the corresponding experimental data are shown. The spectral positions of the resonances of the L1 and L2 modes are especially emphasized by the magenta and cyan dashed lines, respectively. In (d), the natural frequencies of the nanodimer are denoted by the red, green, and blue circles, with their corresponding natural modes shown in the insets. The calculated and experimental extinction spectra for the nanodimer are shown in (e) and (f). The spectral shifts between the real part of the natural frequencies and the line position of the simulated resonances are emphasized by the red arrows.

quality factor  $Q$  of the resonance of the Ni nanopatch's natural modes. The quality factor  $Q$  of the resonance of a natural mode can be approximately estimated by [5]

$$Q_{\alpha} = \frac{\omega_{\alpha r}}{2\omega_{\alpha i}} \quad (15)$$

where  $\omega_{\alpha r}$  and  $\omega_{\alpha i}$  are the real and imaginary parts of the  $\alpha$ th natural frequency. Thus, for the natural frequencies with similar real parts, the Ni nanopatch's natural frequencies are always further away from the real frequency axis, i.e., have a bigger imaginary part, than for the Au nanopatch, as can be seen in Fig. 7(a). Physically, such an observation is the consequence of the fact that nickel is a much more lossy material than gold at optical frequencies [34]. For the dimer structure, by utilizing X polarized light, grazing X polarized light and Y polarized light, the L1, L2, and L3 modes are excited. Their calculated and experimental extinction spectra are denoted by solid lines in Fig. 7(e) and (f), respectively. Since the L2 mode (i.e., quadrupole mode) has a small net dipole moment, i.e., it is less radiative than the L1 and L3 modes, its resonance

TABLE 1

Natural frequencies for the Au nanopatch with coarse and fine meshes

	1 <sup>st</sup>	2 <sup>nd</sup>	3 <sup>rd</sup>
coarse	273.8 + $j$ 242.0	325.1 + $j$ 346.7	394.5 + $j$ 85.6
fine	272.1 + $j$ 240.7	322.4 + $j$ 342.0	394.4 + $j$ 88.4

has a narrower resonance in the extinction spectrum [see Fig. 7(e) and (f)] and thus a smaller imaginary part of its corresponding natural frequency [see the green circle in Fig. 7(d)].

Notice that, owing to fabrication inaccuracies and the oversimplification of the substrate effect in our simulations, the simulated results are systematically blue-shifted with respect to the experimental spectra (see the simulations when the substrate is taken into account in the Supporting Information). It is also worth discussing the mismatch between the real part of the natural frequencies and the spectral position of resonances. First of all, we calculate the natural frequencies with finer meshes (see Fig. S1 in the Supporting Information). Here, we tabulate the results for an Au nanopatch in Table 1 (see the results for an Au nanopatch and an Au nanodimer in the Supporting Information). As can be readily seen, there appears to be a very small difference between the natural frequencies calculated from the denser meshes and the ones from the coarse meshes. Therefore, it can be concluded that the mismatch is not due to the coarseness of the mesh. Actually, the shift can be attributed to the imaginary part of the natural frequencies as in the discussions on the spectral shift in near and far field peak intensities of plasmonic nanoantennas [35]–[41]. Further, as shown in (9), all natural modes that are coupled to the incident light contribute to the response of a nanoantenna. Especially, the incident light does not only couple with the natural mode whose natural frequency has a positive real part, i.e.,  $\omega_\alpha = \omega_{\alpha r} + j\omega_{\alpha i}$ , but also with the mode whose natural frequency has a negative real part, i.e.,  $\omega_\alpha = -\omega_{\alpha r} + j\omega_{\alpha i}$ . The above observation may constitute another possible reason for the shift. Besides, since the extinction/scattering cross section is in fact a power spectrum, we must realize the fact that the excited modes are not energetically orthogonal (they are only orthogonal in a quasi-inner product sense) [5], [28], [29], [42]. Hence, these natural modes can interfere with each other [43] and add extra shift between the position of the natural resonance and the spectral peak.

## 5. Conclusion

In conclusion, in order to numerically find the natural frequencies and the natural modes for a nanoantenna, we propose a new parameter, the characteristic term, as a substitute for the matrix determinant. This characteristic term is obtained by doing the *QR* decomposition of the impedance matrix generated by a Volumetric Method of Moments (V-MoM) algorithm. Based on the phase angle information derived from the *Q* matrix and the argument principle, we can determine the number of natural frequencies within a given region of the complex frequency plane. Further, with the help of root finding algorithms, the position of natural frequencies can be located. The proposed procedure is qualitatively confirmed by both numerical results from V-MoM calculation and experimental evidence. The proposed method offers the possibility to numerically extract the most intrinsic aspects, i.e., the natural frequencies and natural modes, of arbitrary nanoantennas. Since natural frequencies and natural modes in general control the steady state response as in (9) and transient response [1] of a nanoantenna, our method may have a direct impact on the design of composite nanostructures [18], nanoantenna arrays [44], and ultrafast time-domain microscopy [45].

## References

- [1] C. E. Baum, "On the singularity expansion method for the solution of electromagnetic interaction problem," Air Force Weapon Lab., Wright-Patterson Air Force Base, OH, USA, Interaction Note 88, 1971.

- [2] L. Marin and R. W. Latham, "Analytical properties of the field scattered by a perfectly conducting, finite body," Northrop Corp. Lab., Pasadena, CA, USA, Interaction Note 92, 1972.
- [3] R. F. Harrington, *Time-Harmonic Electromagnetic Fields*. New York, NY, USA: McGraw-Hill, 1961.
- [4] L. Marin and R. W. Latham, *Field Computation by Moments Methods*, IEEE Press, 1993.
- [5] X. Zheng, V. Volskiy, V. K. Valev, G. A. E. Vandenbosch, and V. V. Moshchalkov, "Line position and quality factor of plasmonic resonances beyond the quasi-static limit: A full-wave eigenmode analysis route," *IEEE J. Sel. Topics Quantum Electron.*, vol. 19, no. 3, p. 4600908, May/June 2013.
- [6] G. A. E. Vandenbosch and A. R. Van de Capelle, "Mixed-potential integral expression formulation of the electric field in a stratified dielectric medium application to the case of a probe current source," *IEEE Trans. Antennas Propag.*, vol. 40, no. 7, pp. 806–817, Jul. 1992.
- [7] F. J. Demuyne, G. A. E. Vandenbosch, and A. R. V. de Capelle, "The expansion wave concept part i: Efficient calculation of spatial Green's functions in a stratified dielectric medium," *IEEE Trans. Antennas Propag.*, vol. 46, no. 3, pp. 397–406, Mar. 1998.
- [8] M. Vrancken and G. A. E. Vandenbosch, "Hybrid dyadic-mixed-potential and combined spectral-space domain integral-equation analysis of quasi-3-D structures in stratified media," *IEEE Trans. Microw. Theory Tech.*, vol. 51, no. 1, pp. 216–255, Jan. 2003.
- [9] Y. Schols and G. A. E. Vandenbosch, "Separation of horizontal and vertical dependencies in a surface/volume integral equation approach to model quasi 3D structures in multilayered media," *IEEE Trans. Antennas Propag.*, vol. 55, no. 4, pp. 1086–1094, Apr. 2007.
- [10] G. A. E. Vandenbosch, V. Volskiy, N. Verellen, and V. V. Moshchalkov, "On the use of the method of moments in plasmonic applications," *Radio Sci.*, vol. 46, no. 5, pp. RS0E02-1–RS0E02-6, Oct. 2011.
- [11] X. Zheng *et al.*, "Volumetric method of moments and conceptual multilevel building blocks for nanotopologies," *IEEE Photon. J.*, vol. 4, no. 1, pp. 267–282, Feb. 2012.
- [12] *IEEE Standard for Floating-Point Arithmetic*, IEEE Std. 754-2008, pp. 1–70, Aug. 2008.
- [13] C. A. Balanis, *Antenna Theory: Analysis and Design*. Hoboken, NJ, USA: Wiley, 2012.
- [14] V. K. Valev *et al.*, "The role of chiral local field enhancements below the resolution limit of second harmonic generation microscopy," *Opt. Exp.*, vol. 20, no. 1, pp. 256–264, Jan. 2012.
- [15] V. K. Valev *et al.*, "Hotspot decorations map plasmonic patterns with the resolution of scanning probe techniques," *Phys. Rev. Lett.*, vol. 106, no. 22, pp. 226803-1–226803-4, Jun. 2011.
- [16] V. K. Valev *et al.*, "Distributing the optical near field for efficient field-enhancements in nanostructures," *Adv. Mater.*, vol. 24, no. 35, pp. OP208–OP215, Sep. 2012.
- [17] N. Verellen, P. Van Dorpe, D. Vercrusysse, G. A. E. Vandenbosch, and V. V. Moshchalkov, "Dark and bright localized surface plasmons in nanocrosses," *Opt. Exp.*, vol. 19, no. 12, pp. 11 034–11 051, Jun. 2011.
- [18] N. Verellen *et al.*, "Fano resonances in individual coherent plasmonic nanocavities," *Nano Lett.*, vol. 9, no. 4, pp. 1663–1667, Apr. 2009.
- [19] D. Vercrusysse *et al.*, "Unidirectional side scattering of light by a single-element nanoantenna," *Nano Lett.*, vol. 13, no. 8, pp. 3843–3849, Aug. 2013.
- [20] S. Zhang, D. A. Genov, Y. Wang, M. Liu, and X. Zhang, "Plasmon-induced transparency in metamaterials," *Phys. Rev. Lett.*, vol. 101, no. 4, pp. 047401-1–047401-4, Jul. 2008.
- [21] X. Zheng *et al.*, "Interacting plasmonic nanostructures beyond the quasi-static limit: A circuit model," *Opt. Exp.*, vol. 21, no. 25, pp. 31 105–31 118, Dec. 2013.
- [22] L. Novotny, "Effective wavelength scaling for optical antennas," *Phys. Rev. Lett.*, vol. 93, no. 26, pp. 266802-1–266802-4, Jun. 2007.
- [23] L. Ahlfors, *Complex Analysis*, New York NY, USA: McGraw-Hill, 1979.
- [24] A. W. Glisson and D. R. Wilton, "Simple and efficient numerical methods for problems of electromagnetic radiation and scattering from surfaces," *IEEE Trans. Antennas Propag.*, vol. AP-28, no. 5, pp. 593–603, Sep. 1980.
- [25] S. M. Rao, D. R. Wilton, and A. W. Glisson, "Electromagnetic scattering by surfaces of arbitrary shape," *IEEE Trans. Antennas Propag.*, vol. AP-30, no. 3, pp. 409–418, May 1982.
- [26] B. K. Singaraju, D. V. Giri, and C. E. Baum, "Further developments in the application of contour integration to the evaluation of the zeros of analytic functions and relevant computer programs," Air Force Weapons Lab., Albuquerque, NM, USA, Math. Note 42, 1976.
- [27] F. M. Tesche, "On the singularity expansion method as applied to electromagnetic scattering from thin-wires," Air Force Weapon Lab., Wright-Patterson Air Force Base, OH, USA, Interaction Note 102, 1971.
- [28] A. G. Ramm, "Theoretical and practical aspects of singularity and Eigenmode expansion methods," *IEEE Trans. Antennas Propag.*, vol. AP-28, no. 6, pp. 897–901, Nov. 1980.
- [29] A. G. Ramm, "Mathematical foundations of the singularity and eigenmode expansion methods (SEM and EEM)," *J. Math. Anal. Appl.*, vol. 86, no. 2, pp. 562–591, Apr. 1982.
- [30] R. A. Horn and C. R. Johnson, *Matrix Analysis*. Cambridge, U.K.: Cambridge Univ. Press, 1985.
- [31] C. E. Baum, *The Singularity Expansion Method in Electromagnetic: A Summary Survey and Open Questions*, Akron, OH, USA: SUMMA Foundation, 2012.
- [32] K. G. Murty, *Linear Programming*. Hoboken, NJ, USA: Wiley, 1983.
- [33] P. Rocca, G. Oliveri, and A. Massa, "Differential evolution as applied to electromagnetics," *IEEE Antennas Propag. Mag.*, vol. 53, no. 1, pp. 38–49, Feb. 2011.
- [34] E. D. Palik, *Handbook of Optical Constants of Solids*. Amsterdam, The Netherlands: Elsevier, 1998.
- [35] B. J. Messinger, K. U. von Raben, R. K. Chang, and P. W. Barber, "Local fields at the surface of noble-metal microspheres," *Phys. Rev. B, Condens. Matter*, vol. 24, no. 2, pp. 649–657, Jul. 1981.
- [36] S. Bruzzone, M. Malvaldi, G. P. Arrighini, and C. Guidotti, "Near-field and far-field scattering by bimetallic nanoshell systems," *J. Phys. Chem. B*, vol. 110, no. 23, pp. 11 050–11 054, Jun. 2006.
- [37] N. K. Grady, N. J. Halas, and P. Nordlander, "Influence of dielectric function properties on the optical response of plasmon resonant metallic nanoparticles," *Chem. Phys. Lett.*, vol. 399, no. 1–3, pp. 167–171, Nov. 2004.

- [38] B. Ross and L. Lee, "Comparison of near- and far-field measures for plasmon resonance of metallic nanoparticles," *Opt. Lett.*, vol. 34, no. 7, pp. 896–898, Apr. 2009.
- [39] J. Zuloaga and P. Nordlander, "On the energy shift between near-field and far-field peak intensities in localized plasmon systems," *Nano Lett.*, vol. 11, no. 3, pp. 1280–1283, Mar. 2011.
- [40] J. Chen *et al.*, "Plasmonic nickel nanoantennas," *Small*, vol. 7, no. 16, pp. 2341–2347, Aug. 2011.
- [41] M. A. Kats, N. Yu, P. Genevet, Z. Gaburro, and F. Capasso, "Effect of radiation damping on the spectral response of plasmonic components," *Opt. Exp.*, vol. 19, no. 22, pp. 21 748–21 753, Oct. 2011.
- [42] G. W. Hanson and A. B. Yakovlev, *Operator Theory for Electromagnetics: An Introduction*. New York, NY, USA: Springer-Verlag, 2002.
- [43] N. Verellen *et al.*, "Mode parity-controlled fano- and Lorentz-like line shapes arising in plasmonic nanorods," *Nano Lett.*, vol. 14, no. 5, pp. 2322–2329, May 2014.
- [44] D. Dregely *et al.*, "3D optical Yagi-Uda nanoantenna array," *Nat. Commun.*, vol. 2, no. 4, pp. 267, Apr. 2010.
- [45] D. Brinks, M. Castro-Lopez, R. Hildner, and N. F. van Hulst, "Plasmonic antennas as design elements for coherent ultrafast nanophotonics," *Proc. Nat. Acad. Sci. USA*, vol. 110, no. 46, pp. 18 386–18 390, Nov. 2013.